Fatty-Acid Monolayers at the Nematic/Water Interface: Phases and Liquid-Crystal Alignment

Andrew D. Price and Daniel K. Schwartz*

Department of Chemical and Biological Engineering, University of Colorado, Boulder, Colorado 80309-0424

Received: September 22, 2006; In Final Form: December 6, 2006

The two-dimensional (2D) phases of fatty-acid monolayers (hexadecanoic, octadecanoic, eicosanoic, and docosanoic acids) have been studied at the interface of a nematic liquid crystal (LC) and water. When observed between crossed polarizers, the LC responds to monolayer structure owing to mesoscopic alignment of the LC by the adsorbed molecules. Similar to Langmuir monolayers at the air/water interface, the adsorbed monolayer at the nematic/water interface displays distinct thermodynamic phases. Observed are a 2D gas, isotropic liquid, and two condensed mesophases, each with a characteristic anchoring of the LC zenithal tilt and azimuth. By varying the monolayer temperature and surface concentration we observe reversible first-order phase transitions from vapor to liquid and from liquid to condensed. A temperature-dependent transition between two condensed phases appears to be a reversible swiveling transition in the tilt azimuth of the monolayer. Similar to monolayers at the air/water interface, the temperature of the gas/liquid/condensed triple-point temperature increased by about 10 °C for a two methylene group increase in chain length. However, the absolute value of the triple-point temperatures are depressed by about 40 °C compared to those of analogous monolayers at the air/water interface. We also observe a direct influence by the LC layer on the mesoscopic and macroscopic structure of the monolayer by analyzing the shapes and internal textures of gas domains in coexistence with a 2D liquid. An effective anisotropic line tension arises from elastic forces owing to deformation of the nematic director across phase boundaries. This results in the deformation of the domain from circular to elongated, with a distinct singularity. The LC elastic energy also gives rise to transition zones displaying mesoscopic realignment of the director tilt or azimuth between adjacent regions with a sudden change in anchoring.

Introduction

While monolayers of amphiphilic molecules at the air/water interface (Gibbs or Langmuir monolayers) have been studied extensively by a number of experimental techniques, investigations of monolayers at the liquid−liquid interface have remained fairly limited.[1−4] Molecular level organization at this interface has been particularly difficult to study because of the buried and deformable nature of the interface.[5] As a special class of liquid−liquid interfaces, the interface between an aqueous phase and a nematic liquid crystal (LC) provides a convenient experimental geometry for studying the organization of adsorbed molecules. The LC phase possesses long-range orientational order that couples to the interface, a phenomenon known as surface anchoring. Monolayer packing, tilt of the alkyl chains, and lateral organization, all dependent on the temperature, surface pressure, and surface density of the monolayer, are presumed to influence LC anchoring. Thus, optical properties of the LC can be used as a tool to investigate molecular order in the interfacial layer.[6]

Anchoring orients the LC director at the boundary of interest and is defined by two angles: zenithal and azimuthal (Figure 1).[7] The zenithal angle may be planar (director aligned parallel to the interface), homeotropic (director aligned perpendicular to the interface), or tilted (director aligned at an intermediate angle). This angle is commonly defined as 0° for homeotropic and 90° for planar alignment. The azimuthal angle is related to the projection of the LC director onto the interface. The optical anisotropy of a nematic LC molecule creates a difference in the refractive indices of light polarized parallel and perpendicular to the molecular director. This is known as birefringence. When viewed between a set of crossed polarizers, birefringence in the plane of polarization results in the transmission of light. The magnitude of birefringence is determined by thickness of the liquid crystal layer and the average zenithal angle of the LC director.[8] The intensity of the transmitted light also depends on the relation between the azimuthal alignment and the polarizer/analyzer. Azimuthal alignment perpendicular to the direction of the polarizer or analyzer extinguishes all light; alignment 45° to the polarizer and analyzer allows for maximum intensity. Of particular interest is the relation between molecular orienta-

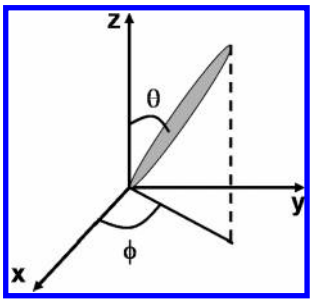

Figure 1. Zenithal angle, θ, is the angle between the LC director and the z-axis. Azimuthal angle, ϕ, is the angle between the director projection on the $x-y$ plane and the x-axis.

* To whom correspondence should be addressed. E-mail: daniel.schwartz@colorado.edu. Phone: 303-735-0240. Fax: 303-492-4341.

10.1021/jp066228b CCC: $37.00
Published on Web 01/13/2007

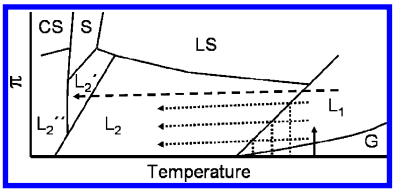

Figure 2. Schematic generalized phase diagram for fatty-acid monolayers at the air/water interface.[30] The solid arrow shows an isothermal increase in surface pressure above the triple point. The dashed arrow shows a phase progression from isotropic liquid through condensed mesophases with decreasing temperature. The dotted arrows show the positive correlation between surface pressure and the temperature of L_1/L_2 phase transitions.

tion in an interfacial layer (e.g., packing density, tilt, orientation order) and nematic alignment.

Previous studies by Abbott and workers have shown that surfactants adsorbed at the aqueous−nematic interface at high enough density cause homeotropic alignment of the LC layer.[9−11] The reversible adsorption of surfactant molecules at the interface caused a continuous transition in LC orientation from planar to homeotropic.[11] Subsequent work concluded that interactions between the aliphatic tails of the surfactant and the LCs anchor the molecules at the interface.[9,10] A thermodynamic model by Rey considered interfacial energies to connect areal density of the surfactant at the interface to LC orientation.[12] The model predicted a discontinuous transition in LC orientation that proceeded from planar to homeotropic to random orientation with increasing concentration of surfactant at the interface. This was in contrast to the Abbott studies which determined a continuous transition in LC orientation. Unlike detergent systems where the amphiphile is highly soluble in the aqueous subphase, phospholipids remain irreversibly adsorbed to the interface.[13,14] Phospholipid adsorption caused a transition from planar to homeotropic that appeared discontinuous, with homeotropic areas growing and fusing until a uniform homeotropic appearance was achieved.[14] This result hints at the influence of the monolayer phase on the anchoring of the liquid crystal layer.

The phase behavior of Langmuir monolayers at the air/water interface has been extensively studied. The most well-studied monolayers are *n*-alkanoic acids, that is, fatty acids, whose phases are characterized by surface density, tilt of the alkyl chains, and lateral organization.[15−21] Our current understanding of two-dimensional fatty-acid monolayer phases began with thermodynamic measurements (isotherms)[22] and was refined through extensive investigations using polarized fluorescence microscopy[15,18,23−25] and Brewster angle microscopy (BAM)[15,26] to delineate phase boundaries by observing changes in probe solubility and optical contrast respectively. X-ray diffraction studies (see review by Kaganer et al.)[27] established the molecular arrangement of monolayers directly on the water surface, for example, the unit cell dimensions and tilt directions of the monolayer phases.[28,29] Figure 2, adapted from Knobler[30] shows a generalized phase diagram for fatty-acid monolayers at the air/water interface. Similar phases are present for all chain lengths from 14 to 24 with the abscissa shifted 7−12 K to the right for each subtraction of two methylene groups. In addition to 2D vapor (G) and isotropic liquid (L_1) phases, a variety of mesophases (L_2, L_2', LS, S) and crystalline phases (L_2'', CS), both tilted and untilted, have been observed and characterized.

Fatty-acid monolayers display both continuous and discontinuous phase transitions[15,16,18] that may significantly influence the mesoscopic alignment of an adjacent LC film via changes to surface anchoring. Hiltrop and Stegemeyer investigated amphiphilic monolayers transferred to solid supports, Langmuir−Blodgett (LB) monolayers, at controlled packing densities and temperatures.[31,32] They observed the homeotropic alignment of the LC by a fatty-acid monolayer at low-packing density and temperatures near the nematic to isotropic transition. Cooling well below a critical temperature caused the LC layer to become increasingly tilted. Fang et al. created LB films of monoglycerides and demonstrated that the molecular tilt azimuth in the monolayer induced azimuthal orientation in nematic LCs.[6] A recent study by Collins et al. demonstrated the ability of loosely packed fatty-acid monolayers to align a LC layer homeotropically.[33] In their study, a mixture of eicosanoic acid and a nematic LC was transferred onto a solid support. The LC was believed to interpenetrate the fatty-acid molecules and induce homeotropic alignment in a LC cell. Studies using transferred LB monolayers involve some uncertainty regarding possible structural changes during transfer relative to the monolayer at the air/water interface. For example, there have been observations suggesting that laterally homogeneous, loosely packed monolayers at the air/water interface often undergo a structural transition during LB transfer, resulting in an inhomogeneous monolayer consisting of dense patches coexisting with dilute regions.[34−42] For studies that involve 2D phase behavior, it is desirable to avoid this additional LB transfer step whenever possible.

The present study aims to further the understanding of amphiphilic monolayer phases at the nematic/water interface as a function of surface concentration and temperature. The results will be discussed in three sections. The first section will discuss the qualitative appearance of the phases as viewed using a polarizing microscope. The birefringence colors and rotational anisotropy observed can be described in terms of the zenithal and azimuthal anchoring at the nematic/water interface, a strong indication that the monolayer phase affects LC anchoring. The second section will characterize the phase boundaries of fatty-acid monolayers containing progressively longer alkyl chains. The evidence suggests a correspondence between the phases at the nematic/water interface and phases at the air/water interface. The final section focuses on gas domains present in the isotropic L_1 phase. The shapes of these domains and the apparent textures within them are influenced by the elastic forces of the adjacent nematic. In other words, in certain cases the nematic layer cannot simply be seen as a passive reporter of monolayer structure, it can also affect the monolayer on mesoscopic and macroscopic length scales.

Experimental Details

LC Film Preparation. Borosilicate glass slides were cleaned with a fresh piranha solution composed of 30% aqueous H_2O_2 and concentrated H_2SO_4 (1:3 v/v) for 1 h at 70 °C. (**Warning: piranha solution reacts strongly with organic compounds and should be handled with extreme caution; do not store solution in closed containers.**) An octadecyltriethoxysilane (OTES) (Gelest, Inc.) self-assembled monolayer (SAM) was deposited on the glass following the procedure described by Walba et al.[43] Briefly, clean glass slides were rinsed with acetone and toluene and submerged in a solution of toluene, OTES, and butylamine (200:3:1 v/v) for 30 min at 60 °C. Following, the glass slides were rinsed with toluene, dried with a stream of nitrogen, and stored under a vacuum at room temperature for 24 h prior to use. This produced a surface with a water contact angle of ∼95° as measured optically by the sessile drop method with a goniometer; sufficient to induce homeotropic alignment of the liquid crystal (LC). The slides were cut into small rectangles measuring approximately 0.75 in. × 0.50 in.

The LC material used was E7 ($n_\perp = 1.57$, $n_\parallel = 1.73$, Merck Ltd.), a four-component LC mixture of cyanobiphenyls and a cyanoterphenyl with a nematic to isotropic (N−I) transition temperature of 60 °C.[8] The LC was drawn into a 25 μm capillary tube and used to fill a TEM grid via capillary action by contacting the capillary tube to a TEM grid laying flat on a rectangle of SAM-coated glass. The TEM grid (SPI Supplies) used was a gold-coated copper, square mesh grid with hole sizes of 205 μm. Following the introduction of the LC into the grid, the LC was heated above its N−I transition temperature and slowly cooled back to room temperature. This resulted in a LC layer of approximately 20 μm in thickness.

Preparation of Fatty-Acid Solutions. Hexadecanoic acid, octadecanoic acid, eicosanoic acid, and docosanoic acid (Sigma 99% grade) were used without further purification. Fatty acids were dissolved in chloroform to a concentration of 20−30 mg/mL. Hexadecanoic acid and octadecanoic acid were deposited at the interface by creating a dispersion of vesicles that fuse to the interface. To prepare these dispersions, the fatty acids dissolved in chloroform were dispensed into a glass vial, dried under a stream of nitrogen, and placed under vacuum for at least 2 h. The dried fatty acids were resuspended in an aqueous solution of 25 mM Tris, 50 mM NaCl, and 1 mM ethylenediaminetetraacetic acid (EDTA) that was adjusted to a pH of 8.0 and to a concentration of 200 μM. Subsequent sonication of the mixtures at 70 °C for 10 min created a clear solution of primarily small unilamellar vesicles. The solutions were used within 24 h of their preparation. The existence of deprotonated fatty acids (pKa $\approx$ 6.0) at pH 8.0 aided significantly in their adsorption at the interface.

Eicosanoic acid, docosanoic acid, and sometimes octadecanoic acid were suspended in an alcohol-based solution because of their tendency to form large aggregates in aqueous solutions. The fatty acids dissolved in chloroform were dispensed into glass vials, dried under a stream of nitrogen, and placed under vacuum for at least 2 h. Dried fatty acids were resuspended in a mixture of ethyl alcohol and an aqueous solution of 10 mM potassium acid phthalate, 50 mM NaCl, and 0.5 mM EDTA adjusted to a pH of 3.9 (9:1 v/v) to a range of concentrations between 70 and 900 μM.

Formation of Fatty-Acid Monolayers. Monolayers were formed using the aqueous solutions by filling a chamber slide (Lab-Tek) with vesicle suspension and heating to 40 °C. LC-filled TEM grids on SAM-coated glass were submerged in the solution for 15−120 min to achieve the desired degree of monolayer coverage. The solution was held constant at 40 °C throughout the adsorption process. A cover was placed on the chamber to limit evaporation. For ethanolic solutions, layer formation was achieved by dispensing 1 μL of the solution onto the LC-filled grids and allowing the drops to evaporate (approximately 10 s). Subsequently the grids were submerged in a chamber slide containing an aqueous solution of 25 mM tris, 50 mM NaCl, and 1 mM EDTA adjusted to a pH of 8.0 and heated to 40 °C. The chain length used was determined by the temperatures of the phase transitions and, in the case of fatty-acid adsorption experiments, solubility in an aqueous solution.

Polarized Light Microscopy. The LC orientation and textures were observed using plane-polarized light with an Olympus BH2-UMA microscope modified for transmission mode incorporating crossed polarizers. The chamber slide containing the LC setup was placed on a rotating stage with an attached custom heating and cooling stage. The stage was located between the polarizers. All images were captured using a COHU 2232 CCD video camera mounted on the microscope and positioned so its x and y axes were aligned with those of the polarizer and analyzer. Homeotropic orientation was determined by the absence of transmitted light during a full 360° rotation of the sample. In the absence of homeotropic orientation, zenithal tilt angle at the nematic/water interface was determined by comparing the observed colors to those on a Michel−Levy chart.[44] This yielded the birefringence, from which we were then able to determine $\theta_{n/w}$, the zenithal angle of the LC director at the nematic/water interface, from the following equation:

$$\Delta n_e = \frac{1}{\theta_{n/w} - \theta_{n/SAM}} \int_{\theta_{n/SAM}}^{\theta_{n/a}} \frac{n_\parallel n_\perp \, d\theta}{\sqrt{n_\parallel^2 \cos^2\theta + n_\perp^2 \sin^2\theta}} - n_\perp$$

where Δn_e was the effective average birefringence, $n_\parallel$ was the index of refraction for E7 parallel to the optical axis, and $n_\perp$ was the index of refraction for E7 perpendicular to the optical axis. $\theta_{n/SAM}$ was the zenithal angle of the LC director at the nematic/SAM interface and was assumed to always have a value of 0 (homeotropic anchoring). The azimuthal angle was determined by rotating the sample to extinction.

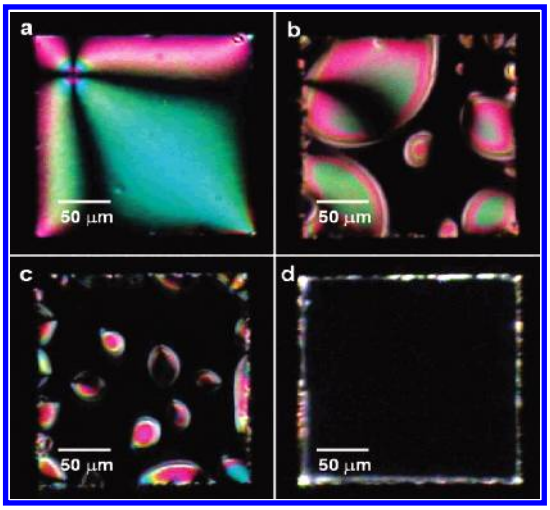

Figure 3. Polarizing microscope images of a nematic LC in contact with a 200 μM hexadecanoic acid solution at $T = 40.0$ °C. The acid gradually adsorbed, increasing the interfacial concentration: (a) time = 0, (b) time = 20 min, (c) time = 35 min, and (d) time = 70 min.

Results

Fatty-Acid Adsorption. Immediately following immersion of the LC-filled grid into the aqueous dispersion of hexadecanoic acid vesicles, we observed light green and pink effective birefringence colors (Figure 3a), indicative of a high effective birefringence with zenithal tilt angles of approximately 78° at the nematic/water interface, a measurement in close agreement with that previously measured for 4′-pentyl-4-cyanobiphenyl (5CB) at the nematic/water interface in the absence of adsorbed amphiphiles.[10] Brush textures, usually present as four extinction lines emanating from a central defect, are commonly observed in nematics with random azimuthal anchoring. Adsorption of fatty acids from vesicles at the interface caused the surface concentration of the adsorbed monolayer to increase as represented schematically by the solid arrow in Figure 2; the associated progression of the LC appearance is presented in Figure 3. At sufficiently high temperatures, the increase in surface concentration was accompanied by the appearance of regions exhibiting homeotropic alignment (Figure 3b). Here the LC director was aligned perpendicular to both the nematic/SAM

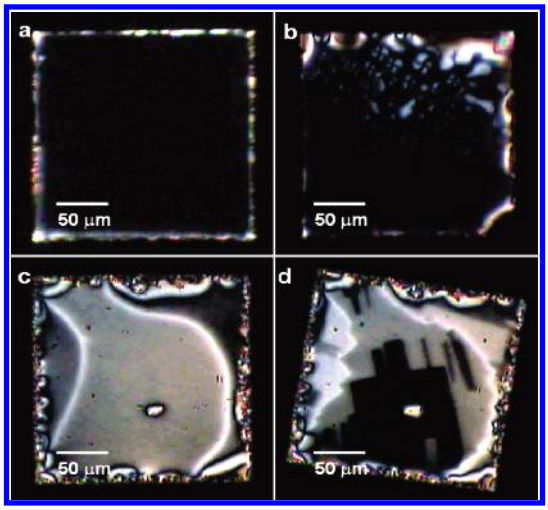

Figure 4. Polarizing microscope images of a nematic liquid crystal in contact with an eicosanoic acid monolayer: (a) $T = 40.0$ °C, (b) $T = 25.4$ °C, (c) $T = 13.0$ °C, and (d) $T = 10.6$ °C.

and nematic/water interfaces allowing for an undistorted zenithal alignment of the LC throughout the LC layer. In analogy with previous studies on surfactants at the nematic/water interface, these homeotropic regions may represent a column of LC that is in contact with a region of monolayer with a relatively high surface concentration (i.e., a 2D liquid).[14] These regions often originated near the grid boundaries and fused, creating coexistence between homeotropically aligned LC and tilted LC regions (Figure 3b,c) which are believed to represent isotropic liquid and gas phases, respectively. It is worth noting that the birefringent regions are not circular, a result which will be discussed later. The homeotropic regions continued to grow with increasing adsorption until the entire grid hole was homeotropic (Figure 3d), an observation in agreement with those of Abbott et al. for surfactants and phospholipids.[9,13,14]

Monolayer Temperature. Similar to the situation for hexadecanoic acid illustrated in Figure 3, adsorbed eicosanoic acid monolayers caused homeotropic alignment of the LC layer over the entire grid hole at high temperatures and surface densities (Figure 4a). Lowering the sample temperature (see dashed arrow in Figure 2) resulted in the appearance of birefringent regions, indicating a tilted anchoring at the monolayer surface. These regions often appeared as dim white or gray circular regions with a pinwheel texture (Figure 4b). With decreasing temperature, the birefringent regions coarsened and merged, becoming large, distinct domains with uniform zenithal and azimuthal alignment (Figure 4c). These domains were stable over some range of temperature; however, at a lower temperature (typically greater than 10 °C below the homeotropic-to-tilted transition) a sudden change of texture was observed. This second transition was characterized by a rearrangement of the existing domains and azimuthal angles accompanied by the emergence of angular and/or striped domains and kinked boundaries (Figure 4d). This phase transition was reversible with a hysteresis of approximately 1.5 °C between heating and cooling transitions. Figure 5 shows the reversibility of this transition for docosanoic acid. The domains of the higher temperature phase (left column) are regenerated following transition, though with some drift in their position. The striped domains of the lower temperature phase (right column) do not stay constant each cycle; however, the larger scale texture appears to be related to the texture of the higher temperature phase. The phases presented in Figure 5 exhibited rotational anisotropy indicating a fixed azimuthal angle of the LC director within a given domain (Figure 6). Dark

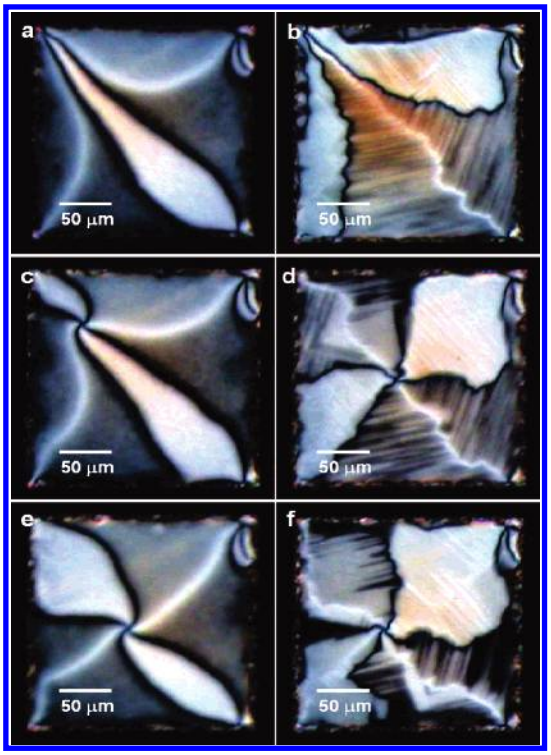

Figure 5. Polarizing microscope images of a reversible transition between higher temperature (a,c,e) and lower temperature (b,d,f) condensed mesophases for docosanoic acid monolayers at the nematic/water interface.

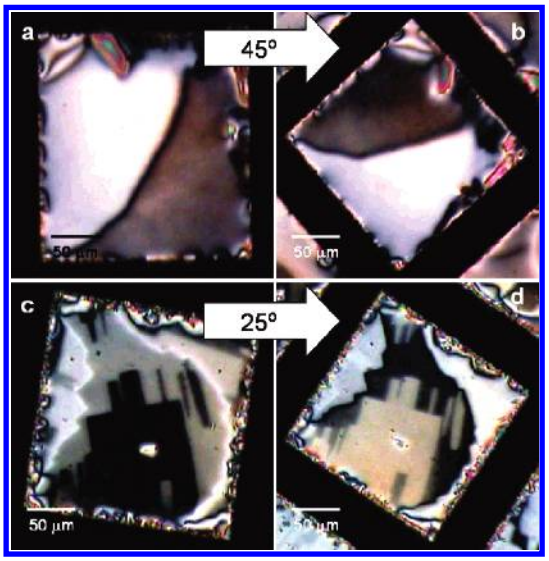

Figure 6. Polarizing microscope images show azimuthal anchoring by the condensed mesophases which cause the light intensity of the domains to vary with rotation. The arrows indicate the degree of clockwise rotation between the images: (a,b) the higher temperature condensed phase (L_2); (c,d) the lower temperature condensed phase (L_2').

domains indicate an azimuthal anchoring angle parallel to the analyzer or polarizer direction. The brighter the domain, the nearer the azimuthal anchoring angle is to being 45° relative to the analyzer and polarizer direction. We suggest that the tilted anchoring that gives rise to the effective birefringence observed in Figures 4 and 5 is due to contact between the LC and anisotropic (probably tilted) condensed monolayer phases. The reversible behavior shown in Figure 5 suggests a transition between two different tilted condensed monolayer phases.

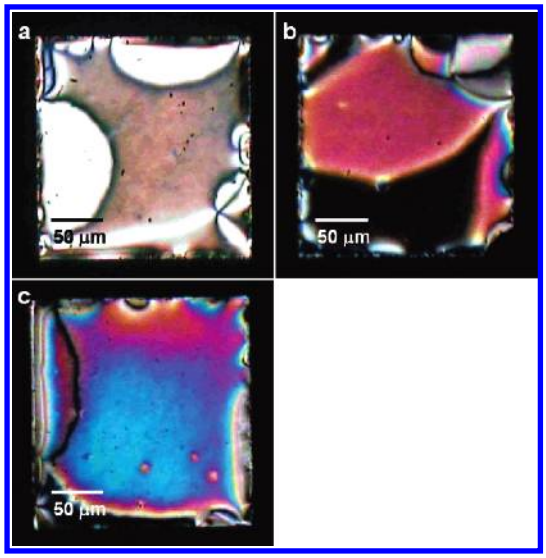

Figure 7. Polarizing microscope images of eicosanoic acid monolayers at the nematic/water interface showing the effect of surface concentration on cell birefringence. All the images were obtained at 13.7 ± 0.4 °C. The homeotropic-to-tilted transitions occurred at (a) 32.8 °C (highest surface concentration), (b) 25.4 °C (intermediate surface concentration), and (c) 21.9 °C (lowest surface concentration).

Monolayer Surface Density. The surface concentration of eicosanoic acid was systematically increased by varying the concentration of the ethanolic deposition solutions progressively from 100 to 700 μM. We have no direct measure of surface concentration; however, we observed a systematic correlation between the concentration of deposition solution and the temperature at which birefringent domains were first observed during cooling (Figure 4b). This is consistent with expectations given the positive slope of the L_1/L_2 coexistence line as shown in Figure 2. Significant variations were observed from hole to hole in the same grid. Apparently spreading and evaporation of the deposition solutions do not deposit the molecules uniformly over the surface. Therefore, we determined that the actual homeotropic-to-tilted transition temperature in a given grid hole was the most reliable indicator of surface concentration in that hole.

Figure 7 shows the effect of surface concentration on the appearance of the nematic LC anchored by condensed phases of eicosanoic acid monolayers. Different surface concentrations of eicosanoic acid were deposited on LC-filled grids at room temperature. Following evaporation of the deposition solution, the grids were immersed in buffer at 40 °C. All concentrations were high enough to cause uniform homeotropic alignment. The sample shown in Figure 7a had the highest surface concentration; those shown in Figure 7 parts b and c were at successively lower concentrations. Upon cooling, the transition from homeotropic to tilted anchoring occurred at successively lower temperatures, consistent with the expected surface concentration trends. For the samples in Figure 7, parts a, b, and c, the homeotropic-to-tilted transitions occurred at 32.8 °C, 25.4 °C, and 21.9 °C, respectively. All images were obtained at T = 13.7 ± 0.4 °C. On the basis of the Michel−Levy colors, one can see that the magnitude of the cell birefringence is greater for lower surface concentrations. On the basis of the effective birefringence colors, the zenithal anchoring angles were calculated to be 39 ± 4°, 45 ± 2°, and 53 ± 2° for Figure 7, parts a, b, and c, respectively.

Triple-Point Temperatures. Ethanolic solutions of 70−100 μM of octadecanoic, eicosanoic, and docosanoic acids were deposited onto the LC layer at high temperatures to create low-surface-density monolayers in gas/L_1 phase coexistence (Figure 8a). The temperature was then slowly lowered until condensed domains were first observed (Figure 8b). This temperature, the triple-point temperature, is where gas, isotropic liquid, and a condensed phase coexist in equilibrium. Further lowering of the temperature caused the homeotropic regions to disappear until only gas/condensed phase coexistence remained (Figure 8c). Figure 9 shows the triple-point temperature as a function of chain length increase for the three fatty acids. Each increase of two methylene groups increased the triple-point temperature by approximately 10 K, in good agreement with the trend at the air/water interface.[45]

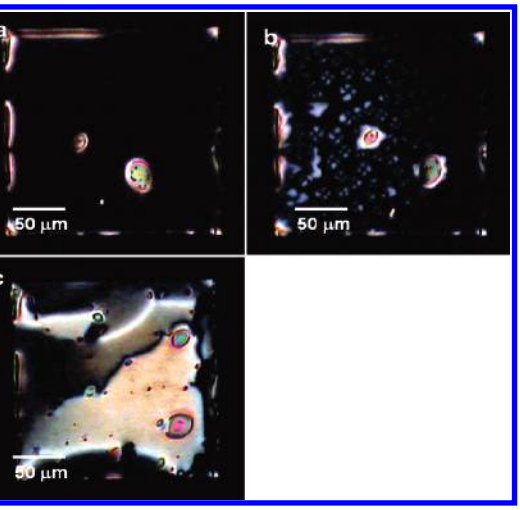

Figure 8. Polarizing microscope images of eicosanoic acid monolayers at the nematic/water interface as a function of decreasing temperature, a−c. (a) T = 26.4 °C; gas and L_1 phases are observed. (b) T = 19.8 °C; small L_2 domains are also observed along with gas and L_1. This is the triple point. (c) T = 16.1 °C; below the triple point, the L_1 phase vanishes.

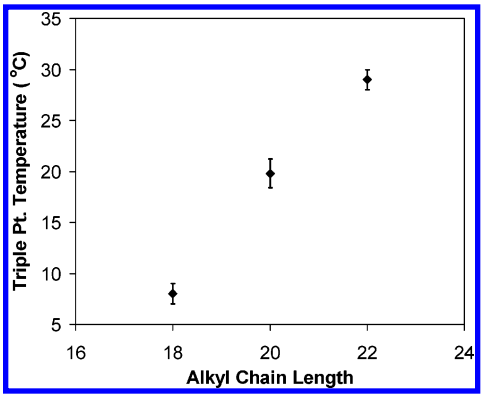

Figure 9. Triple-point temperatures for octadecanoic, eicosanoic, and docasanoic acid monolayers at the nematic/water interface.

Discussion

Characterization of Monolayer Phases. Measurements of the LC cell birefringence, the director azimuth, and the optical texture were sensitive to the phase of the absorbed fatty-acid monolayers. It is expected that in all cases, the aliphatic tails of the fatty-acid molecules are in contact with the hydrophobic LC phase. Viewed with the polarizing microscope, each phase possessed distinct characteristics that allowed us to identify it as either an isotropic gas, a 2D liquid, or a condensed mesophase. The LC characteristics for gas, isotropic liquid, and condensed mesophases are summarized in Table 1. A two-dimensional gas phase with negligible molecular density is

TABLE 1: Monolayer Phases Observed and Their Associated LC Anchoring Characteristics

phase	effective birefringence	zenithal angle at nematic/water interface	azimuthal anchoring?
gas	high	78°	no
isotropic liquid	none	0	
condensed mesophase	low	18−45°	yes

expected to have the same anchoring characteristics as a pure aqueous boundary. Here the fatty-acid molecules are scattered at the interface and have no significant interactions with each other or the LC phase. Figure 3a shows a LC-filled grid immediately following immersion in an aqueous dispersion of fatty-acid vesicles. The LC appearance is characterized by a high effective birefringence and brush textures, indicative of random azimuthal anchoring suggesting a 2D gas phase.

The increased adsorption of fatty acids from vesicles at the interface increased the surface concentration of the adsorbed monolayer which, at temperatures above the triple point, caused regions of homeotropic alignment to appear (Figure 3b−d). Though the molecular-scale interactions responsible for LC anchoring remain poorly understood, past studies have suggested that interdigitation of LC molecules into fatty-acid monolayers homeotropically anchored the molecules upon compression.[46] We label the monolayer phase that causes this homeotropic alignment L_1, in analogy with the 2D liquid phase observed in fatty-acid Langmuir monolayers above the triple point (also sometimes called LE). The L_1 phase involves 2D liquidlike order of fatty-acid headgroups and disordered but interacting tails. The sequence of images in Figure 3 is consistent with a first-order transition from gas to L_1 with increasing surface concentration.

As shown in Figure 2, a decrease in temperature for a Langmuir monolayer in the L_1 phase caused a phase transition into a condensed phase, in particular the L_2 phase. An analogous transition was observed at the nematic/water interface. As the temperature was lowered from the L_1 phase, small birefringent regions appeared. Isolated domains of this new phase often displayed distinctive shapes and textures, such as boojums or stars that are reminiscent of textures seen in hexatic mesophases of Langmuir monolayers.[30] Figure 10 shows isolated L_2 phase domains surrounded by L_1 phase. The continuous variation of the tilt azimuth inside the boojums in particular (Figure 10b), provides strong evidence that the phase is a mesophase and not a 2D crystal. The "pinwheel" defects (Figure 10a) are not directly analogous to previous observations in Langmuir monolayers, although they are related to "star" defects. These are typically six-segmented circles, however in these very small domains, it is likely that the nematic phase would effectively broaden the sharp boundaries within the domain so fine details could not be seen. In general, where sharp orientational transitions occur across any domain boundary, broader transition zones are observed because LC reorientation takes place over a mesoscopic range owing to the energy required for elastic deformation of the nematic director. This can also be observed between L_2 domains with different azimuthal orientations (Figure 6). As the temperature was lowered further, the domains coarsened and coalesced eventually displaying uniform zenithal and azimuthal alignment (Figure 4c−d). The domains had distinct boundaries and low effective birefringence values when compared to the effective birefringence of the gas phase. The zenithal angles at the nematic/water interface generally ranged from 18 to 45°.

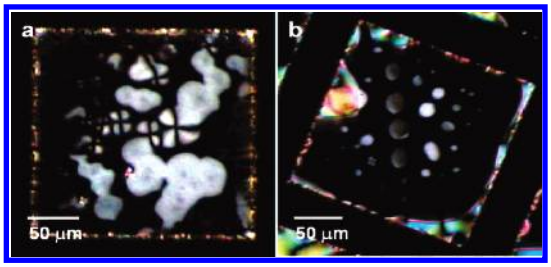

Figure 10. Polarizing microscope images of L_1/L_2 phase coexistence. Chiral pinwheel domains and boojum domains are visible in images a and b, respectively.

Each condensed phase domain defined a particular azimuthal anchoring direction (see Figure 6). This suggests a correspondence with the tilted mesophases of Langmuir monolayers (L_2, L_2', and Ov). We see no evidence of the untilted mesophases under accessible conditions. Multiple domains often existed in one grid hole, each having a preferred azimuthal anchoring. The domain boundaries were meandering and fluid in the L_2 phase, similar to observations of Langmuir monolayers using BAM. It was also observed in the L_2 phase that greater surface concentration resulted in a decrease in the zenithal anchoring angle. This is reminiscent of the behavior of the L_2 phase in Langmuir monolayers, where the molecular tilt angle decreases with increasing surface pressure.[15,16] If this analogy is sound, this suggests that the zenithal anchoring angle may be directly correlated to the molecular tilt within the condensed monolayer phase. At low temperatures, a transition was observed between the L_2 phase and another tilted mesophase. The appearance of this phase was qualitatively similar to that of the L_2 phase; however, domain boundaries were typically composed of straight line segments and sharp kinks, in contrast with the curved L_2 phase domain boundaries. The exact structure of the fatty-acid monolayer in these condensed phases at the aqueous/nematic interface is not known, but the shapes, textures, and LC orientation of the observed domains suggests a correspondence with the similarly labeled condensed phases at the air/water interface.

It should be mentioned that our studies were performed at a pH of 8.0, a pH where the majority of fatty-acid molecules were deprotonated in solution. Numerous studies at the air/water interface have indicated the phase behavior of fatty-acid monolayers remains unchanged for pH values less than 9.0.[47−49] The pK_a values for fatty acids in a monolayer state were measured to be markedly greater than that of a solution state though the reason for this remains unclear.[47] Attempts to carry out our studies at a lowered pH of 4.0 caused our monolayer to collapse as the temperature was lowered. Interestingly, monolayer collapse manifested itself as well-defined faceted crystals similar to those previously observed in collapsed Langmuir films of fatty acids.[50]

Phase Behavior at the Nematic/Water Interface. As previously discussed, the phase of an adsorbed monolayer reflects the current state of the monolayer surface pressure and temperature for the given interface. Between phases exists a boundary where a first or higher-order transition occurs. All the transitions observed were reversible, although sometimes with significant hysteresis. The observation of a triple point provides a characteristic singular temperature for a given system. Figure 9 graphs the dependence of the triple-point temperature on fatty-acid chain length. The 10 K drop in triple-point temperature per each subtraction of two methylene groups is in agreement with the triple-point trend measured at the air/water interface. Indeed even bulk-phase transition temperatures display

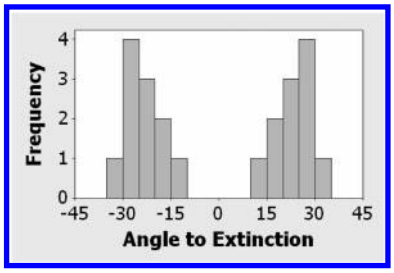

Figure 11. Rotation of the alkyl chain tilt for the swivel transition between the two observed condensed phases. Positive values are clockwise rotations, negative values are counterclockwise rotations.

a similar trend within a homologous series of *n*-alkyl derivatives. However, the actual triple-point temperatures were nearly 40 °C lower than the triple-point temperatures measured for octadecanoic, eicosanoic, and docosanoic acids respectively at the air/water interface (44 °C, 57 °C, and 67 °C respectively).[45] It seems likely that the shift of the melting transition to dramatically lower temperatures must be due to intermolecular interactions between fatty-acid and LC molecules. However, it is not clear whether the effect is mainly due to short-range interactions because of the hydrophobic nature of the LC phase, or to the nematic elasticity. As an example of the former mechanism, one might expect the interdigitation of fatty-acid chains and LC molecules might reduce the molar enthalpy of melting. On the other hand, since the $L_2 \rightarrow L_1$ transition results in a change from tilted to homeotropic anchoring, the elastic energy of the nematic phase must be considered as well. It would be interesting to compare the analogous triple-point temperatures at the aqueous/oil interface, where short-range interactions would be similar to those with the nematic phase, but long-range elastic forces would be lacking.

A second phase transition occurred from one tilted condensed phase to another as the temperature of the eicosanoic and docosanoic monolayers was lowered well beyond their L_1/L_2 transition temperatures (Figure 4d). We will label the higher temperature and lower temperature condensed phases as L_2 and L_2', respectively, in analogy with 2D condensed mesophases observed in fatty-acid Langmuir monolayers. The L_2' phase is characterized by kinked boundaries and angular or striped domains. These kinks are indicative of a strongly anisotropic interfacial tension between tilt domains.[15] Figure 5 shows the reversibility of the L_2/L_2' transition. L_2 domains are regenerated following heating of the L_2' phase while the striped and angular domains of the L_2' phase appear random for each transition cycle. Similar observations have been made regarding the L_2/L_2' transition in Langmuir monolayers called a "swiveling transition" because it involves a change from nearest-neighbor to next-nearest-neighbor tilt. Thus one might expect that the tilt azimuth might swivel macroscopically by a characteristic angle in each domain. This was, in fact, observed, with equal numbers of domains swiveling clockwise (CW) or counterclockwise (CCW). The observed swiveling angles are collected in Figure 11. Like the L_2 phase, the L_2' phase retains its rotational anisotropy (Figure 6) owing to azimuthal anchoring by the molecular tilt of the monolayer.

Similar to the triple-point temperature trend, the temperatures of the L_2/L_2' transition showed approximately a 10 K decrease in transition temperature for each subtraction of two methylene groups from the alkyl chains. Unlike the L_1/L_2 transition, the L_2/L_2' transition temperature changed little with surface concentration having transition temperatures of 11.3 ± 0.3 °C and 21.7 ± 0.7 °C for eicosanoic and docosanoic acids, respectively, regardless of surface concentration. The lower temperatures of the L_2/L_2' transition at the nematic/water interface are in better agreement with condensed phase-transition temperatures at the air/water interface than are the triple-point temperatures. The reasons discussed earlier for the lower triple-point temperatures at the nematic/water interface are not as relevant for transitions between condensed phases where LC molecules are generally excluded from the monolayers and titled anchoring is present in both phases.

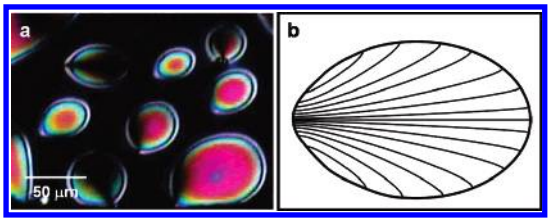

Figure 12. (a) Gas bubbles surrounded by an isotropic liquid phase. (b) Texture of the nematic directors inside the bubbles. The lines show paths of constant azimuth.

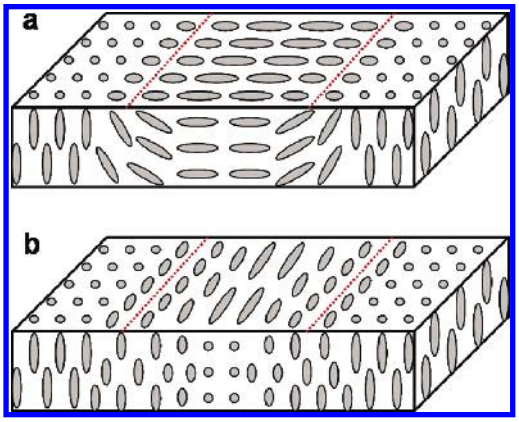

Figure 13. Illustrations of (a) splay deformation and (b) twist deformation of LC molecules at an anchoring boundary. The dashed lines delineate regions of different zenithal anchoring at the interface (top surface) such as occurs at the gas/L_1 phase boundary.

Gas Bubbles in Coexistence with L_1 Phase. Figure 3, parts b and c are images of LC in contact with a hexadecanoic acid monolayer where 2D gas "bubbles" are in coexistence with a continuous L_1 phase. These bubbles appear rounded with cusps at each end, one cusp being more prominent. At equilibrium a bubble takes on a shape that minimizes the system's free energy.[51] At the air/water interface bubbles have a strictly circular boundary as both the gas and L_1 phases are isotropic and lack elastic and line-tension anisotropy.[52] Thus, the anisotropic shape and distinctive internal texture of these bubbles (see Figure 12) must be due to the interaction with the neighboring nematic phase, which has planar anchoring in the gas and homeotropic anchoring in the L_1 phase.

We can formulate a picture of this situation where the boundary between gas and L_1 is characterized by an effective line tension of the bubbles that results not only from the excess free energy between the monolayer phases but also from the nematic elastic forces in the LC phase. There is a rather abrupt change from homeotropic to tilted for the column of LC adjacent to the gas/L_1 monolayer boundary with elastic energy expenditure because of the twist or splay of the nematic director across this boundary (see Figure 13). For nematics, generally twist has a lower energy of deformation than splay.[8] The preference for twist would tend to create a bias for the situation where the LC tilt azimuth lies parallel to the domain boundary as opposed to perpendicular. In general, the actual domain shape and internal

texture will be determined by the situation that minimizes the sum of the effective line tension as well as the in-plane elastic energy.

This problem is closely related to one addressed by Loh and Rudnick,[53] who explored the texture and associated domain shape that results from various forms of boundary and bulk elastic energy in 2D systems. Their analysis of hexatic phase monolayer domains surrounded by an isotropic phase is in many regards similar to our system, if one considers an effective line tension and substitutes the in-plane nematic elasticity for the hexatic elastic free energy. In particular, they consider a line tension of the form $\Gamma(\theta) = 1 + a \cos \theta + b \cos 2\theta$ where θ is the angle between the in-plane component of the director and the domain boundary. They are able to describe the boojum textures typically observed in Langmuir monolayers using a line tension where $b = 0$, that is, the anisotropic part of the line tension goes like $\cos \theta$. This is consistent with the head−tail asymmetry of a surfactant molecule at an interface; one expects a different line tension when the molecule is tilted toward or away from the boundary. The domain shapes and textures shown in Figure 12, however, resemble elongated shapes and textures predicted by Loh and Rodnick when $b \geq a$, that is, the $\cos 2\theta$ term becomes significant in the line tension. Since the anisotropy of the effective line tension in this case is due to nematic LC molecules, which do not have a head−tail asymmetry, this is consistent with expectations. We note that the three-dimensional nature of our system precludes a quantitative comparison to the Loh and Rudnick theory.

Conclusion

This paper demonstrated the use of nematic liquid crystals to investigate the thermodynamic-dependent, bidimensional phases of fatty-acid monolayers adsorbed at the liquid−liquid interface of the nematic and water. Monolayer structure was inferred via phase-dependent anchoring of the LC layer. Zenithal and azimuthal angles of the LC director were measured from effective birefringence and extinction angles respectively. Observed were a 2D gas, isotropic liquid, and two condensed mesophases each displaying characteristic anchoring. The gas phase was characterized by a large zenithal tilt and random azimuthal alignment as noted by the presence of disclination lines. An increase in surface pressure above the triple-point temperature caused a first-order transition to an isotropic liquid (L_1) phase characterized by homeotropic anchoring of the LC. Another first-order phase transition from L_1 to a tilted, condensed phase (L_2) occurred upon lowering the temperature and was characterized by anchoring angles in the 18−45° degree range and a fixed azimuthal angle over large domains. Further lowering the temperature of a monolayer in the L_2 phase caused an apparent swiveling transition in monolayer tilt to a second condensed phase (L_2') characterized by angular and/or striped domains with anchoring similar to the L_2 phase. The zenithal tilt of the condensed phases was inversely correlated to the monolayer surface concentration.

A comparison of gas/L_1/L_2 triple-point temperatures between monolayers at the air/water and nematic/water interfaces revealed both similarities and differences. Triple-point temperatures for octadecanoic, eicosanoic, and docosanoic acids showed approximately a 10 K decrease for each subtraction of two methylene groups from the alkyl chains, in agreement with the trend previously measured at the air/water interface. In contrast, absolute temperatures of the triple points were significantly depressed at the nematic/water interface in comparison with those at the air/water interface. Both short- and long-range interactions of the monolayer with the LC are suspected of contributing to the depressed triple-point temperatures.

Analysis of gas bubbles in the L_1 phase during a first-order phase transition shows a direct influence by the LC layer on the mesoscopic and macroscopic structure of the monolayer. An elongated bubble shape was determined to be due to anisotropy in an effective line tension arising from the deformation of the nematic director. A mathematical analysis of anisotropic 2D domains was able to partially account for the shape and texture observed for the bubbles. This suggests the LC layer is not simply a passive reporter of the adsorbed monolayer but is an active participant in determining monolayer structure.

Acknowledgment. This work was supported by the National Science Foundation (Award No. CHE-0349547) and the Liquid Crystal Materials Research Center (NSF MRSEC, Award No. DMR-0213918). A.P. acknowledges support from a Department of Education GAANN fellowship.

References and Notes

(1) Messmer, M. C.; Conboy, J. C.; Richmond, G. L. *J. Am. Chem. Soc.* **1995**, *117*, 8039.
(2) Lee, L. T.; Langevin, D.; Farnoux, B. *Phys. Rev. Lett.* **1991**, *67*, 2678.
(3) Grubb, S. G.; Kim, M. W.; Rasing, T.; Shen, Y. R. *Langmuir* **1988**, *4*, 452.
(4) Conboy, J. C.; Messmer, M. C.; Richmond, G. L. *J. Phys. Chem. B* **1997**, *101*, 6724.
(5) Lockwood, N. A.; Abbott, N. L. *Curr. Opin. Colloid Interface Sci.* **2005**, *10*, 111.
(6) Fang, J. Y.; Gehlert, U.; Shashidar, R.; Knobler, C. M. *Langmuir* **1999**, *15*, 297.
(7) Rasing, T.; Musevic, I. *Surfaces and Interfaces of Liquid Crystals*; Springer: Berlin, 2004.
(8) Dunmur, D.; Fukuda, A.; Luckhurst, G. R. *Physical properties of liquid crystals: nematics*; INSPEC, Institution of Electrical Engineers: London, 2001.
(9) Lockwood, N. A.; de Pablo, J. J.; Abbott, N. L. *Langmuir* **2005**, *21*, 6805.
(10) Brake, J. M.; Mezera, A. D.; Abbott, N. L. *Langmuir* **2003**, *19*, 8629.
(11) Brake, J. M.; Abbott, N. L. *Langmuir* **2002**, *18*, 6101.
(12) Rey, A. D. *Langmuir* **2004**, *20*, 11473.
(13) Brake, J. M.; Daschner, M. K.; Luk, Y. Y.; Abbott, N. L. *Science* **2003**, *302*, 2094.
(14) Brake, J. M.; Daschner, M. K.; Abbott, N. L. *Langmuir* **2005**, *21*, 2218.
(15) Riviere, S.; Henon, S.; Meunier, J.; Schwartz, D. K.; Tsao, M. W.; Knobler, C. M. *J. Chem. Phys.* **1994**, *101*, 10045.
(16) Ramos, S.; Castillo, R. *J. Chem. Phys.* **1999**, *110*, 7021.
(17) Ocko, B. M.; Kelley, M. S.; Nikova, A. T.; Schwartz, D. K. *Langmuir* **2002**, *18*, 9810.
(18) Moore, B.; Knobler, C. M.; Broseta, D.; Rondelez, F. *J. Chem. Soc., Faraday Trans. 2* **1986**, *82*, 1753.
(19) Kaganer, V. M.; Indenbom, V. L. *J. Phys. II* **1993**, *3*, 813.
(20) Chi, L. F.; Gleiche, M.; Fuchs, H. *Langmuir* **1998**, *14*, 875.
(21) Alonso, C.; Zasadzinski, J. A. *J. Phys. Chem. B* **2006**, *110* 22185.
(22) Stallberg-Stenhagen, S.; Stenhagen, E. *Nature (London)* **1945**, *156*, 239.
(23) Schwartz, D. K.; Knobler, C. M. *J. Phys. Chem.* **1993**, *97*, 8849.
(24) Moy, V. T.; Keller, D. J.; Gaub, H. E.; Mcconnell, H. M. *J. Phys. Chem.* **1986**, *90*, 3198.
(25) Knobler, C. M.; Desai, R. C. *Annu. Rev. Phys. Chem.* **1992**, *43*, 207.
(26) Overbeck, G. A.; Mobius, D. *J. Phys. Chem.* **1993**, *97*, 7999.
(27) Kaganer, V. M.; Mohwald, H.; Dutta, P. *Rev. Mod. Phys.* **1999**, *71*, 779.
(28) Kaganer, V. M.; Peterson, I. R.; Kenn, R. M.; Shih, M. C.; Durbin, M.; Dutta, P. *J. Chem. Phys.* **1995**, *102*, 9412.
(29) Kaganer, V. M.; Loginov, E. B. *Phys. Rev. E: Stat. Phys., Plasmas, Fluids, Relat. Interdiscip. Top.* **1995**, *51*, 2237.
(30) Knobler, C. M. *Il Nuovo Cimento* **1998**, *20*, 2095.
(31) Hiltrop, K.; Stegemeyer, H. *Liq. Cryst. Ordered Fluids* **1984**, *4*.

(32) Hiltrop, K.; Stegemeyer, H. *Ber. Bunsen-Ges. Phys. Chem.* **1978**, *82*, 884.
(33) Collins, J.; Funfschilling, D.; Dennin, M. *Thin Solid Films* **2006**, *496*, 601.
(34) Tippmann-Krayer, P.; Moehwald, H.; L'Vov, Y. M. *Langmuir* **1991**, *7*, 2298.
(35) Steitz, R.; Mitchell, E. E.; Peterson, I. R. *Thin Solid Films* **1991**, *205*, 124.
(36) Sikes, H. D.; Woodward, J. T.; Schwartz, D. K. *J. Phys. Chem.* **1996**, *100*, 9093.
(37) Sikes, H. D.; Schwartz, D. K. *Langmuir* **1997**, *13*, 4704.
(38) Shih, M. C.; Peng, J. B.; Huang, K. G.; Dutta, P. *Langmuir* **1993**, *9*, 776.
(39) Rana, F. R.; Mautone, A. J.; Dluhy, R. A. *Appl. Spectrosc.* **1993**, *47*, 1015.
(40) Mikrut, J. M.; Dutta, P.; Ketterson, J. B.; Macdonald, R. C. *Phys. Rev. B; Condens. Matter Mater. Phys.* **1993**, *48*, 14479.
(41) Fang, J. Y.; Knobler, C. M. *J. Phys. Chem.* **1995**, *99*, 10425.
(42) Chi, L. F.; Fuchs, H.; Johnston, R. R.; Ringsdorf, H. *Thin Solid Films* **1994**, *242*, 151.
(43) Walba, D. M.; Liberko, C. A.; Korblova, E.; Farrow, M.; Furtak, T. E.; Chow, B. C.; Schwartz, D. K.; Freeman, A. S.; Douglas, K.; Williams, S. D.; Klittnick, A. F.; Clark, N. A. *Liq. Cryst.* **2004**, *31*, 481.
(44) Robinson, P. C.; Davidson, M. W. Michel−Levy Interference Color Chart; http://www.microscopyu.com/articles/polarized/michel-levy.html, 2006.
(45) Peterson, I. R.; Brzezinski, V.; Kenn, R. M.; Steitz, R. *Langmuir* **1992**, *8*, 2995.
(46) Barmentlo, M.; Vrehen, Q. H. F. *Chem. Phys. Lett.* **1993**, *209*, 347.
(47) Oishi, Y.; Takashima, Y.; Suehiro, K.; Kajiyama, T. *Langmuir* **1997**, *13*, 2527.
(48) Johann, R.; Vollhardt, D.; Mohwald, H. *Langmuir* **2001**, *17*, 4569.
(49) Johann, R.; Vollhardt, D. *Mater. Sci. Eng., C* **1999**, *8*−*9*, 35.
(50) Valdes-Covarrubias, M. A.; Cadena-Nava, R. D.; Vasquez-Martinez, E.; Valdez-Perez, D.; Ruiz-Garcia, J. *J. Phys.: Condens. Matter* **2004**, *16*, S2097.
(51) Fang, J. Y.; Teer, E.; Knobler, C. M.; Loh, K. K.; Rudnick, J. *Phys. Rev. E: Stat. Phys., Plasmas, Fluids, Relat. Interdiscip. Top.* **1997**, *56*, 1859.
(52) Rudnick, J.; Bruinsma, R. *Phys. Rev. Lett.* **1995**, *74*, 2491.
(53) Loh, K. K.; Rudnick, J. *Phys. Rev. Lett.* **1998**, *81*, 4935.